

MAGNETICALLY DRIVEN PRECESSION OF WARPED DISKS AND MILLI-HERTZ VARIABILITIES IN ACCRETING X-RAY PULSARS

AKIKO SHIRAKAWA AND DONG LAI

Center for Radiophysics and Space Research, Cornell University, Ithaca, NY 14853

Email: shirak,dong@astro.cornell.edu

Draft version December 2, 2024

ABSTRACT

The inner region of the accretion disk around a magnetized neutron star is subjected to magnetic torques that induce warping and precession of the disk. These torques arise from interactions between the stellar field and the induced electric currents in the disk. We carry out a global analysis of warping/precession modes in a viscous accretion disk, and show that under a wide range of conditions typical of accreting X-ray pulsars, the magnetic warping torque can overcome viscous damping and make the mode grow. The warping/precession modes are concentrated near the inner edge of the disk (at the magnetosphere-disk boundary), and can give rise to variabilities or quasi-periodic oscillations (QPOs) in the X-ray/UV/optical fluxes from X-ray pulsars. We examine the observed properties of mHz QPOs in several systems (such as 4U 1626-67), and suggest that some hitherto unexplained QPOs are the results of magnetically driven disk warping/precession.

Subject headings: accretion, accretion disks – stars: neutron – stars: magnetic fields – pulsars – binaries: close

1. INTRODUCTION

Disk accretion onto a magnetic star occurs in a variety of astrophysical contexts, including accreting neutron stars, white dwarfs and pre-main-sequence stars (e.g., Frank et al. 1992). The basic picture of disk–magnetosphere interaction is well-known: at large radii the disk is unaffected by the stellar magnetic field; a somewhat sudden transition occurs when the stellar field disrupts the disk at the magnetospheric boundary (where the magnetic and plasma stresses balance), and channels the plasma onto the polar caps of the star. A large number of theoretical papers have been written on the subject of the interaction between accretion disks and magnetized stars (e.g., Pringle & Rees 1972; Ghosh & Lamb 1979, 1992; Aly 1980; Anzer & Börner 1980, 1983; Lipunov et al. 1981; Wang 1987, 1995; Aly & Kuipers 1990; Spruit & Taam 1993; Shu et al. 1994; van Ballegooijen 1994; Lovelace et al. 1995, 1998; Li, Wickramasinghe & Rüdiger 1996; Campbell 1997; Lai 1998; Terquem & Papaloizou 2000), but numerical study of this problem is still in its infancy (e.g., Hayashi et al. 1996; Miller & Stone 1997; Goodson et al. 1997; Fendt & Elstner 2000). Outstanding issues remain, including the efficiency of field dissipation in/outside the disk, whether the disk excludes the stellar field by diamagnetic currents or the field can penetrate a large fraction of the disk, whether the threaded field remains closed (connecting the star and the disk) or becomes open by differential shearing, and whether/how magnetically driven wind is launched from the disk or the magnetosphere/corotation boundary.

Many previous theoretical papers have, for simplicity, adopted the idealized geometry in which the magnetic axis, the spin axis and the disk angular momentum are aligned. However, in Lai (1999), it was shown that under quite general conditions, the stellar magnetic field can induce warping in the inner disk and make the disk precess around the spin axis (see §2). Such magnetically driven warping and precession open up new possibilities for the

dynamical behaviors of disk accretion onto magnetic stars. In Shirakawa & Lai (2001) we have studied these effects in weakly magnetized accreting neutron stars and showed that the magnetic warping/precession effects may explain several observed features of low-frequency quasi-periodic oscillations in low-mass X-ray binaries.

In this paper we study global, magnetically driven warping/precession modes of inner disks of highly magnetized ($B \sim 10^{12}$ G) neutron stars (NSs), as in accreting X-ray pulsars (§2 and §3). Such study is the first step toward understanding the observational manifestations of the magnetic warping/precession effects. We are motivated by the observations of the milli-Hertz quasi-periodic oscillations (QPOs) in a number of X-ray pulsars (see Table 1 in §4 and references therein). Of particular interest is the recent detection of the 1 mHz optical/UV oscillations in 4U 1626-67 (Chakrabarty et al. 2001). In §4, we use the results of §3 and suggest that magnetically driven disk warping and precession naturally explain this and some other mHz variabilities observed in X-ray pulsars.

2. MAGNETICALLY DRIVEN WARPING/PRECESSION AND ITS GLOBAL MODES

The inner region of the accretion disk onto a rotating magnetized central star is subjected to magnetic torques that induce warping and precession of the disk (Lai 1999). These magnetic torques result from the interactions between the accretion disk and the stellar magnetic field. Depending on how the disk responds to the stellar field, two different kinds of torque arise: (i) If the vertical stellar magnetic field B_z penetrates the disk, it gets twisted by the disk rotation to produce an azimuthal field $\Delta B_\phi = \mp\zeta B_z$ that has different signs above and below the disk (ζ is the azimuthal pitch of the field line and depends on the dissipation in the disk), and a radial surface current K_r results. The interaction between K_r and the stellar B_ϕ gives rise to a vertical force. While the mean force (averaging over the azimuthal direction) is zero, the un-

even distribution of the force induces a net *warping torque* which tends to misalign the angular momentum of the disk with the stellar spin axis. (ii) If the disk does not allow the vertical stellar field (e.g., the rapidly varying component of B_z due to stellar rotation) to penetrate, an azimuthal screening current K_ϕ will be induced on the disk. This K_ϕ interacts with the radial magnetic field B_r and produces a vertical force. The resulting *precessional torque* tends to drive the disk into retrograde precession around the stellar spin axis.

In general, both the magnetic warping torque and the precessional torque are present. For small disk tilt angle β (the angle between the disk normal and the spin axis), the precession angular frequency and warping rate at radius r are given by (see Lai 1999)¹

$$\Omega_p(r) = \frac{\mu^2}{\pi^2 r^7 \Omega(r) \Sigma(r) D(r)} F(\theta), \quad (1)$$

$$\Gamma_w(r) = \frac{\zeta \mu^2}{4\pi r^7 \Omega(r) \Sigma(r)} \cos^2 \theta, \quad (2)$$

where μ is the stellar magnetic dipole moment, θ is the angle between the magnetic dipole axis and the spin axis, $\Omega(r)$ is the orbital angular frequency, and $\Sigma(r)$ is the surface density of the disk. The dimensionless function $D(r)$ is given by

$$D(r) = \max \left(\sqrt{r^2/r_{\text{in}}^2 - 1}, \sqrt{2H(r)/r_{\text{in}}} \right), \quad (3)$$

where $H(r)$ is the half-thickness and r_{in} is the inner radius of the disk. The function $F(\theta)$ depends on the dielectric property of the disk. We can write

$$F(\theta) = 2f \cos^2 \theta - \sin^2 \theta, \quad (4)$$

so that $F(\theta) = -\sin^2 \theta$ if only the spin-variable vertical field is screened out by the disk ($f = 0$), and $F(\theta) = 3 \cos^2 \theta - 1$ if all vertical field is screened out ($f = 1$). In reality, f lies between 0 and 1. For concreteness, we shall set $F(\theta) = -\sin^2 \theta$ in the following.

For accretion-powered X-ray pulsars, the inner disk radius r_{in} is given by the magnetosphere radius r_m :

$$r_{\text{in}} \equiv \eta \left(\frac{\mu^4}{G M \dot{M}^2} \right)^{1/7} = (3.4 \times 10^8 \text{ cm}) \eta \mu_{30}^{4/7} M_{1.4}^{-1/7} \dot{M}_{17}^{-2/7}, \quad (5)$$

where $M = (1.4M_\odot)M_{1.4}$ is the neutron star mass, $\dot{M} = (10^{17} \text{ g s}^{-1})\dot{M}_{17}$ is the mass accretion rate, $\mu_{30} = \mu/(10^{30} \text{ G cm}^3)$, and $\eta \sim 0.5 - 1$. For typical parameters, the precession frequency is

$$\frac{\Omega_p(r)}{2\pi} = -(11.8 \text{ mHz}) \mu_{30}^2 M_{1.4}^{-1/2} r_8^{-11/2} \times \left[\frac{\Sigma(r)}{10^4 \text{ g cm}^{-2}} \right]^{-1} \left[\frac{D(r)}{0.1} \right]^{-1} \sin^2 \theta, \quad (6)$$

where we have used $\Omega(r) = (GM/r^3)^{1/2}$, and $r_8 = r/(10^8 \text{ cm})$. The warping rate $\Gamma_w(r)$ is of the same order of magnitude as $\Omega_p(r)$.

Since the precession rate $\Omega_p(r)$ depends strongly on r , coupling between different rings is needed to produce a global coherent precession. The coupling can be achieved either by viscous stress or through bending waves (e.g.,

¹ Note that the stellar spin frequency Ω_s does not appear in eqs. (1) & (2) since the variation of the field geometry due to the spin has been averaged out; this is justified because $\Omega_s \gg |\Omega_p|, |\Gamma_w|$.

Papaloizou & Pringle 1983; Papaloizou & Terquem 1995; Larwood et al. 1996; Terquem 1998). In the viscosity dominated regime (i.e., the dimensionless viscosity parameter α greater than H/r), the dynamics of the warps can be studied using the formalism of Papaloizou & Pringle (1983) (see also Pringle 1992; Ogilvie 1999; Ogilvie & Dubus 2001). We model the disk as a collection of rings which interact with each other via viscous stresses. Each ring at radius r has the unit normal vector $\hat{\mathbf{l}}(r, t)$. In the Cartesian coordinates, with the z -axis along the neutron star spin, we write $\hat{\mathbf{l}} = (\sin \beta \cos \gamma, \sin \beta \sin \gamma, \cos \beta)$, with $\beta(r, t)$ the tilt angle and $\gamma(r, t)$ the twist angle. For $\beta \ll 1$, the dynamical warp equation for $\hat{\mathbf{l}}$ (Lai 1999; see Papaloizou & Pringle 1983; Pringle 1992) reduces to an equation for $W(r, t) \equiv \beta(r, t) e^{i\gamma(r, t)}$:

$$\frac{\partial W}{\partial t} - \left[\frac{3\nu_2}{4r} \left(1 + \frac{2r\mathcal{J}'}{3\mathcal{J}} \right) + \frac{3\nu_1}{2r} (\mathcal{J}^{-1} - 1) \right] \frac{\partial W}{\partial r} = \frac{1}{2} \nu_2 \frac{\partial^2 W}{\partial r^2} + i\Omega_p W + \Gamma_w W, \quad (7)$$

where $\mathcal{J}' = d\mathcal{J}/dr$, ν_1 is the usual viscosity, and ν_2 is the viscosity which tends to reduce the disk tilt. We assume that the ratio of ν_2 to ν_1 is constant. In deriving eq. (7), we have used the relations for the radial velocity and surface density: $v_r = -3\nu_1 \mathcal{J}^{-1}/2r$ and $\Sigma = \dot{M}\mathcal{J}/3\pi\nu_1$. The values and functional forms of ν_1 , ν_2 , Ω_p , Γ_w [see eqs. (1) & (2)], and the dimensionless function $\mathcal{J}(r)$ [see eq. (16) below] depend on disk models.

2.1. Power-law Disk Models

To gain insight on the properties of the global warping-precessional modes, we consider power-law disk models, with $\Sigma(r) \propto r^\mu$. We also assume that $D(r) = \text{constant}$, $\mathcal{J}(r) = 1$, $\nu_2/\nu_1 = 1$, and $\Omega(r) \propto r^{-3/2}$ as in the Keplerian flow. Then, from eqs. (1) & (2), we have

$$\Omega_p(r) = \Omega_p(r_{\text{in}}) \left(\frac{r}{r_{\text{in}}} \right)^{-\mu-11/2}, \quad (8)$$

$$\Gamma_w(r) = \Gamma_w(r_{\text{in}}) \left(\frac{r}{r_{\text{in}}} \right)^{-\mu-11/2}. \quad (9)$$

Using the relation $\Sigma = \dot{M}\mathcal{J}/3\pi\nu_1$, the viscosity rate τ_{visc}^{-1} can be written as

$$\tau_{\text{visc}}^{-1}(r) \equiv \frac{\nu_2(r)}{r^2} = \tau_{\text{visc}}^{-1}(r_{\text{in}}) \left(\frac{r}{r_{\text{in}}} \right)^{-\mu-2}. \quad (10)$$

We look for a solution of the form $W(r, t) = e^{i\sigma t} W(r)$ with the complex mode frequency $\sigma (= \sigma_r + i\sigma_i)$. It is convenient to define dimensionless quantities by

$$\hat{\sigma} \equiv \sigma(r_{\text{in}}) \tau_{\text{visc}}(r_{\text{in}}), \quad \hat{\Omega}_p \equiv \Omega_p(r_{\text{in}}) \tau_{\text{visc}}(r_{\text{in}}), \\ \hat{\Gamma}_w \equiv \Gamma_w(r_{\text{in}}) \tau_{\text{visc}}(r_{\text{in}}). \quad (11)$$

Equation (7) then reduces to the dimensionless form:

$$i\hat{\sigma} W - \frac{3}{4x^{\mu+1}} \frac{dW}{dx} = \frac{1}{2x^\mu} \frac{d^2 W}{dx^2} + i \frac{\hat{\Omega}_p}{x^{\mu+11/2}} W + \frac{\hat{\Gamma}_w}{x^{\mu+11/2}} W, \quad (12)$$

where $x \equiv r/r_{\text{in}}$.

It is clear from eq. (12) that, for a given μ , the mode frequency $\hat{\sigma}$ depends only on two dimensionless parameters $\hat{\Omega}_p$ and $\hat{\Gamma}_w$. To solve eq. (12) for the complex eigenfunction $W(x)$ and eigenvalue $\hat{\sigma}$, six real boundary conditions are needed. In our calculation, the disk extends from $x_{\text{in}} = 1$ to $x_{\text{out}} = 50$. For large x and large $|\hat{\sigma}|$, equation (12) can be solved analytically, giving

$$W(x) \propto \exp \left[\frac{2\sqrt{2}}{\mu+2} (i\hat{\sigma})^{1/2} x^{\mu/2+1} \right], \quad (13)$$

where the sign of $(i\hat{\sigma})^{1/2}$ should be chosen so that $W(x) \rightarrow 0$ as $x \rightarrow \infty$. This approximate analytical solution, evaluated at x_{out} , together with its derivative, gives four (real) outer boundary conditions. The inner boundary condition generally takes the form $W'(x_{\text{in}}) = aW(x_{\text{in}})$, with a being a constant. Most of our results in §3 are based on $a = 0$ (corresponding to zero torque at the inner edge of the disk), although we have experimented with different a 's and found that for $|a| \lesssim 1$ similar results are obtained (see Shirakawa & Lai 2001). In numerically searching a mode, we make a guess for the eigenvalue $\hat{\sigma}$ and integrate eq. (12) from x_{out} to x_{in} . Since $W(x)$ changes very rapidly from x_{out} to x_{in} , we rewrite eq. (12) in terms of a new function w defined as $W = e^w$ and use that equation for integration. We find the correct value of $\hat{\sigma}$ that satisfies the boundary conditions using the globally convergent Newton method (Press et al. 1992).

2.2. Middle-Region Solution of the α -Disk

Here we consider the “middle-region” (gas-pressure-and scattering-dominated) solution of the α -disk (Shakra & Sunyaev 1973; Novikov & Thorne 1973) which is relevant to the inner part of the disk in accretion-powered X-ray pulsars. In this model,

$$\Sigma = (7.5 \times 10^3 \text{ g cm}^{-2}) \alpha_{-1}^{-4/5} M_{1.4}^{1/5} \dot{M}_{17}^{3/5} r_8^{-3/5} \mathcal{J}^{3/5}, \quad (14)$$

$$H = (1.0 \times 10^6 \text{ cm}) \alpha_{-1}^{-1/10} M_{1.4}^{-7/20} \dot{M}_{17}^{1/5} r_8^{21/20} \mathcal{J}^{1/5}, \quad (15)$$

where $\alpha = (0.1)\alpha_{-1}$ is the α -viscosity parameter. The dimensionless function $\mathcal{J}(r)$ is given by²

$$\mathcal{J}(r) = 1 - \xi \sqrt{\frac{r_{\text{in}}}{r}}, \quad (16)$$

where ξ is a dimensionless parameter with $0 \leq \xi < 1$ ($\xi = 0$ corresponds to zero net angular momentum transfer across the inner disk, i.e., when the star is in spin equilibrium). Substituting equation (14) into equations (1) and (2), and using $\Omega(r) = (GM/r^3)^{1/2}$, we get

$$\begin{aligned} \Omega_p(r) &= (-9.8 \times 10^{-3} \text{ s}^{-1}) \sin^2 \theta \mu_{30}^2 \alpha_{-1}^{4/5} M_{1.4}^{-7/10} \\ &\quad \times \dot{M}_{17}^{-3/5} r_8^{-49/10} \mathcal{J}(r)^{-3/5} D(r)^{-1}, \end{aligned} \quad (17)$$

$$\begin{aligned} \Gamma_w(r) &= (7.7 \times 10^{-3} \text{ s}^{-1}) \zeta \cos^2 \theta \mu_{30}^2 \alpha_{-1}^{4/5} M_{1.4}^{-7/10} \\ &\quad \times \dot{M}_{17}^{-3/5} r_8^{-49/10} \mathcal{J}(r)^{-3/5}. \end{aligned} \quad (18)$$

Using $\nu_1 = \alpha H^2 \Omega$, the viscosity rate is calculated as

$$\begin{aligned} \tau_{\text{visc}}^{-1}(r) &\equiv \frac{\nu_2(r)}{r^2} = (1.4 \times 10^{-4} \text{ s}^{-1}) \left(\frac{\nu_2}{\nu_1} \right) \alpha_{-1}^{4/5} M_{1.4}^{-1/5} \\ &\quad \times \dot{M}_{17}^{2/5} r_8^{-7/5} \mathcal{J}(r)^{2/5}. \end{aligned} \quad (19)$$

² Magnetic fields threading the disk can modify $\mathcal{J}(r)$ in a model-dependent way (see Lai 1999 for an example). However, the basic feature can still be approximated by eq. (16).

With $W(r, t) = e^{i\sigma t} W(r)$, and using the dimensionless quantities $\hat{\sigma}$, $\hat{\Omega}_p$, and $\hat{\Gamma}_w$ as defined in eq. (11), we can write equation (7) in the dimensionless form:

$$\begin{aligned} i\hat{\sigma}W - \left[\frac{3}{4} \left(1 + \frac{2x\mathcal{J}'}{3\mathcal{J}} \right) + \frac{3\nu_1}{2\nu_2} \left(\frac{1}{\mathcal{J}} - 1 \right) \right] \left(\frac{\mathcal{J}}{x\mathcal{J}_{\text{in}}} \right)^{2/5} \frac{dW}{dx} \\ = \frac{x^{3/5}}{2} \frac{\mathcal{J}^{2/5}}{\mathcal{J}_{\text{in}}^{2/5}} \frac{d^2W}{dx^2} + i \frac{\hat{\Omega}_p}{x^{4.9}} \frac{D_{\text{in}} \mathcal{J}_{\text{in}}^{3/5}}{D \mathcal{J}^{3/5}} W + \frac{\hat{\Gamma}_w}{x^{4.9}} \frac{\mathcal{J}_{\text{in}}^{3/5}}{\mathcal{J}^{3/5}} W, \end{aligned} \quad (20)$$

where $D_{\text{in}} \equiv D(r_{\text{in}})$, $\mathcal{J}_{\text{in}} \equiv \mathcal{J}(r_{\text{in}})$, and $\mathcal{J}' = d\mathcal{J}/dx$. Using eqs. (3), (5), and (15), we can calculate D_{in} as

$$D_{\text{in}} = 0.14 \left(\frac{\eta}{0.5} \right)^{1/40} \mu_{30}^{1/70} \alpha_{-1}^{-1/20} M_{1.4}^{-5/28} \dot{M}_{17}^{13/140} \mathcal{J}_{\text{in}}^{1/10}. \quad (21)$$

Using eqs. (5) & (21) in eqs. (17), (18), & (19), we can calculate $\hat{\Omega}_p$ and $\hat{\Gamma}_w$ as

$$\begin{aligned} \hat{\Omega}_p &= -38.0 \left(\frac{\nu_1}{\nu_2} \right) \left(\frac{\eta}{0.5} \right)^{-141/40} \left(\frac{\sin^2 \theta}{0.5} \right) \mu_{30}^{-1/70} \alpha_{-1}^{1/20} \\ &\quad \times M_{1.4}^{5/28} \dot{M}_{17}^{-13/140} \mathcal{J}_{\text{in}}^{-11/10}, \end{aligned} \quad (22)$$

$$\hat{\Gamma}_w = 21.4 \left(\frac{\nu_1}{\nu_2} \right) \left(\frac{\eta}{0.5} \right)^{-7/2} \left(\frac{\zeta}{5} \right) \left(\frac{\cos^2 \theta}{0.5} \right) \mathcal{J}_{\text{in}}^{-1}. \quad (23)$$

Note that under the assumptions of $\mathcal{J}(x) = 1$ and $D(x) = D_{\text{in}}$, eq. (20) reduces to eq. (12) with $\mu = -0.6$.

3. NUMERICAL RESULTS

3.1. Mode Eigenfunction and Eigenvalue

We first consider the power-law disk models of §2.1. For a given set of parameters $(\mu, \hat{\Omega}_p, \hat{\Gamma}_w)$, equation (12) allows for many eigenmodes. We shall focus on the “fundamental” mode which is more concentrated near the inner edge of the disk and has larger $\hat{\sigma}_r$ (global precession frequency) and smaller $\hat{\sigma}_i$ (damping rate) than any other “higher-order” modes.

Figure 1 shows the tilt angle $\beta(x, t = 0) = |W(x)|$ associated with the modes for different sets of $(\hat{\Omega}_p, \hat{\Gamma}_w)$, all with $\mu = -0.6$ (corresponding to the “middle-region” α -disk with $\mathcal{J}(x) = 1$ and $D(x) = D_{\text{in}}$). We see that as $|\hat{\Omega}_p|$ (note $\hat{\Omega}_p < 0$ due to retrograde precession) and $\hat{\Gamma}_w$ increase, the modes become more concentrated near the inner radius of the disk. This behavior can be understood heuristically: for a given $|\hat{\Omega}_p(r_{\text{in}})|$, a larger $|\hat{\Omega}_p|$ implies smaller viscosity [see eq. (11)], and thus the coupling between different disk radii is reduced, and the mode is less spread.

Figure 2(a) shows the magnitude of the mode frequency ($\hat{\sigma}_r < 0$ due to retrograde precession) $|\hat{\sigma}_r|$ in units of $|\hat{\Omega}_p|$ as a function of $|\hat{\Omega}_p|$ for different values of $\hat{\Gamma}_w$. The ranges of $|\hat{\Omega}_p|$ and $\hat{\Gamma}_w$ are chosen to be from 10 to 1000 to cover possible values of parameters for accretion-powered X-ray pulsars [see eqs. (22) & (23) with $\mathcal{J}_{\text{in}} = 1$]. We include the $\mu = -1.0$ and $\mu = 1.0$ results as well as the “middle region” $\mu = -0.6$ result to show how our results vary with the change of the surface density power-law. We see that $|\hat{\sigma}_r/\hat{\Omega}_p| = |\sigma_r/\Omega_p(r_{\text{in}})|$ always lies between 0.3 to 0.85. The ratio $|\hat{\sigma}_r/\hat{\Omega}_p|$ increases as $|\hat{\Omega}_p|$ and $\hat{\Gamma}_w$ increase. This

is consistent with the behavior of the mode eigenfunction (see Fig. 1) that a larger $|\hat{\Omega}_p|$ and $\hat{\Gamma}_w$ make the mode more concentrated near the inner disk edge.

3.2. Global Warping Instability Criterion

In the absence of magnetic warping torque ($\Gamma_w = 0$), we expect the disk warp to be damped by the viscous stress acting on the differential precession (Ω_p). This “magnetic Bardeen-Petterson effect” (Lai 1999) is analogous to the usual Bardeen-Petterson effect (Bardeen & Petterson 1975), where the combined effects of viscosity and differential Lense-Thirring precession align the rotation axis of the inner disk with the spin axis of the rotating black hole (or rotating, non-magnetic NS). The competition between the magnetically driven warping (Γ_w) and the magnetic Bardeen-Petterson damping can be determined by our global analysis.

Figure 2(b) shows the damping rate $\hat{\sigma}_i$ as a function of $|\hat{\Omega}_p|$ for different values of $\hat{\Gamma}_w$. We see that $\hat{\sigma}_i$ decreases as $\hat{\Gamma}_w$ increases, and becomes negative (implying mode growth) when the ratio $\hat{\Gamma}_w/|\hat{\Omega}_p|$ is sufficiently large. By solving eq. (12) with $\mu = -0.6$, we find that the numerical value of $\hat{\sigma}_i$ can be approximated by

$$\hat{\sigma}_i = -a\hat{\Gamma}_w + b|\hat{\Omega}_p|^{0.6}, \quad (24)$$

with $a \sim (0.5 - 1.0)$ and $b \sim (0.5 - 1.0)$; this result is insensitive to modest change of the surface density power-law ($\mu = -1$ to 1). For the mode to grow ($\hat{\sigma}_i < 0$) we require

$$\hat{\Gamma}_w \gtrsim 2|\hat{\Omega}_p|^{0.6} \iff \text{Global Warping Instability.} \quad (25)$$

Using eqs. (22) and (23), this condition becomes

$$1.6 \left(\frac{\nu_1}{\nu_2} \right)^{0.4} \left(\frac{\eta}{0.5} \right)^{-1.39} \left(\frac{\zeta}{5} \right) \cos^2 \theta (\sin^2 \theta)^{-0.6} \mu_{30}^{0.0086} \times \alpha_{-1}^{-0.03} M_{1.4}^{-0.11} \dot{M}_{17}^{0.056} \mathcal{J}_{\text{in}}^{-0.34} \gtrsim 1 \quad (26)$$

We see that for parameters which characterize X-ray pulsars the mode growth condition can be satisfied, although not always. In general, high (but not unreasonable) ζ (> 1) and small \mathcal{J}_{in} (see §3.3) are preferred to obtain growing modes.

3.3. Effect of $\mathcal{J}(r)$

The results of §3.1–3.2 are based on eq. (12), corresponding to eq. (20) with $D(x) = D_{\text{in}}$ and $\mathcal{J}(x) = 1$. Here we consider the solutions of eq. (20) with the function $\mathcal{J}(x)$ given by eq. (16).

Figure 3 shows the mode frequency $\hat{\sigma}$ as a function of $\mathcal{J}_{\text{in}} = 1 - \xi$ [see eq. (16)] for three different sets of $(\hat{\Omega}_p, \hat{\Gamma}_w)$: $(-38\mathcal{J}_{\text{in}}^{-1.1}, 21\mathcal{J}_{\text{in}}^{-1})$, $(-7.6\mathcal{J}_{\text{in}}^{-1.1}, 38\mathcal{J}_{\text{in}}^{-1})$, and $(-38\mathcal{J}_{\text{in}}^{-1.1}, 43\mathcal{J}_{\text{in}}^{-1})$; these are obtained from eqs. (22) & (23) with $(\sin^2 \theta, \zeta) = (0.5, 5)$, $(0.1, 5)$, and $(0.5, 10)$, respectively, while other parameters being fixed to the standard values [$\eta = 0.5$, $\nu_2/\nu_1 = 1$, $\mu_{30} = 1$, $\alpha_{-1} = 1$, $M_{1.4} = 1$, $\dot{M}_{17} = 1$]. In the calculations, we set $D(x) = D_{\text{in}}$ for simplicity; using the more accurate function $D(x)$ given in eq. (3) only slightly changes the numerical results. We see from Fig. 3 that $|\hat{\sigma}_r/\hat{\Omega}_p|$ is insensitive to the choice of ξ since the most of the dependence on \mathcal{J}_{in} is already absorbed into the definition of $\hat{\Omega}_p$ [see eq. (22)]. We also see that a small \mathcal{J}_{in} tends to increase $\hat{\sigma}_i/|\hat{\Omega}_p|$, although

growing warping modes still exist for a wide range of parameters. We find that the simple global warping instability criteria given in eqs. (25) and (26) can be used for $\mathcal{J}_{\text{in}} > 0.1$. For smaller \mathcal{J}_{in} ($\lesssim 0.1$), $\hat{\sigma}_i$ should be obtained numerically to determine whether the mode grows or gets damped.

4. APPLICATIONS TO MILLI-HERTZ QPO'S IN ACCRETING X-RAY PULSARS

QPOs with frequencies $1 - 100$ mHz have been detected in at least 11 accreting X-ray pulsars (Table 1; see also Boroson et al. 2000). These mHz QPOs are often interpreted in terms of the beat frequency model (BFM; Alpar & Shaham 1985; Lamb et al. 1985) or the Keplerian frequency model (KFM; van der Klis et al. 1987). In the BFM, the observed QPO frequency represents the beat between the Keplerian frequency ν_K at the inner disk radius r_{in} and the NS spin frequency ν_s [i.e., $\nu_{\text{QPO}} = \nu_K(r_{\text{in}}) - \nu_s$]. In the KFM, the QPOs arise from the modulation of the X-rays by some inhomogeneities in the inner disk at the Keplerian frequency [i.e., $\nu_{\text{QPO}} = \nu_K(r_{\text{in}})$]. However, we see from Table 1 that for several sources, more than one QPOs have been detected and the difference in the QPO frequencies is not equal to the spin frequency. Thus it is evident that the KFM and/or the BFM cannot be the whole story. We also note that in both the KFM and the BFM, it is always postulated that the inner disk contain some blobs or inhomogeneities, whose physical origin is unclear.

Here we suggest a “Magnetic Disk Precession Model” (MDPM) for the mHz variabilities and QPOs of accreting X-ray pulsars. The magnetically driven precession of the warped inner disk (outside but close to the magnetosphere boundary) can modulate X-ray/UV/optical flux in several ways: (i) The observed radiation (in UV and optical, depending on r_{in}) from the inner disk due to intrinsic viscous dissipation varies as the angle between the local disk normal vector and the line-of-sight changes during the precession; (ii) The flux of reprocessed UV/optical disk emission visible along our sight also varies as the reprocessing geometry evolves; (iii) Modulation of the X-ray flux arises from regular occultation/obscuration of the radiation from the central NS and magnetosphere by the precessing inner disk. In the MDPM, we identify ν_{QPO} with the global precession frequency driven by the magnetic torques. Our calculations in §3 show that under a wide range of conditions, the warping/precession mode is concentrated near the disk inner edge, and the global mode frequency is equal to $A = 0.3 - 0.85$ (depending on details of the disk structure) times the magnetically driven precession frequency at $r_{\text{in}} = r_m$. Thus we write $\nu_{\text{QPO}} = A|\Omega_p(r_{\text{in}})|/2\pi$. Using eq. (17) together with eqs. (5), (14), and (21), we have (for the α -disk model),

$$\begin{aligned} \nu_{\text{QPO}} &= (15.7 \text{ mHz}) A \sin^2 \theta \mu_{30}^{4/5} \alpha_{-1}^{7/10} \dot{M}_{17}^{-3/5} \\ &\quad \times \left(\frac{r_{\text{in}}}{10^8 \text{ cm}} \right)^{-49/10} \left(\frac{D_{\text{in}}}{0.1} \right)^{-1} \mathcal{J}_{\text{in}}^{-3/5} \\ &= (0.83 \text{ mHz}) A \left(\frac{\eta}{0.5} \right)^{-4.93} \sin^2 \theta \mu_{30}^{-0.81} \\ &\quad \times \alpha_{-1}^{0.85} M_{1.4}^{0.18} \dot{M}_{17}^{0.71} \mathcal{J}_{\text{in}}^{-0.7}. \end{aligned} \quad (27)$$

We also note that the Keplerian frequency at $r = r_{\text{in}} = r_m$ is

$$\nu_K(r_{\text{in}}) = (985 \text{ mHz}) \left(\frac{\eta}{0.5} \right)^{-3/2} \mu_{30}^{-6/7} M_{1.4}^{5/7} \dot{M}_{17}^{3/7}. \quad (28)$$

We see from eq. (27) that the MDPM can produce QPOs with frequencies of order 1 mHz; larger values of ν_{QPO} would require $\mathcal{J}_{\text{in}} \ll 1$ (corresponding to low surface density at r_{in}). The value of \mathcal{J}_{in} depends on details of the physics at the inner edge of the disk, therefore is uncertain. Let $V_r(r_{\text{in}}) = \chi c_s(r_{\text{in}})$, where $V_r = \dot{M}/(2\pi r \Sigma)$ is the radial velocity and $c_s = H\Omega$ is the sound speed of the disk, we find

$$\mathcal{J}_{\text{in}} \simeq 3.1 \times 10^{-4} \chi^{-5/4} \alpha_{-1}^{9/8} M_{1.4}^{-7/16} \dot{M}_{17}^{1/4} \left(\frac{r_{\text{in}}}{10^8 \text{ cm}} \right)^{1/16}. \quad (29)$$

Setting $\chi = 1$ would give the minimum value of \mathcal{J}_{in} .

We now discuss several individual sources.

4.1. 4U 1626+67

The LMXB 4U 1626+67 consists of a $\nu_s = 130$ mHz X-ray pulsar in a 42 min orbit with very low-mass ($\lesssim 0.1 M_{\odot}$) companion (see Chakrabarty 1998). QPOs at 48 mHz (and oscillations at 130 mHz) have been detected simultaneously in X-rays and in the optical/UV band (Shinoda et al. 1990; Chakrabarty 1998; Chakrabarty et al. 2001). Thus it is natural to attribute the optical/UV variability to the reprocessing of the variable X-ray emission in the accretion disk. Since $\nu_s > 48$ mHz, the KFM is problematic because the propeller effect would inhibit accretion when $\nu_s > \nu_K(r_m)$. (It is still possible to ascribe the QPO to Keplerian motion at some radius farther out in the disk, but this is rather ad hoc.) The BFM is a viable alternative for the 48 mHz QPO.

Recent HST observations by Chakrabarty et al. (2001) revealed a strong QPO around 1 mHz (centroid frequency in the range of 0.3–1.2 mHz, and $Q = \nu/\Delta\nu$ of order 10) in the optical/UV band. This QPO is absent in simultaneous X-ray data, and is stronger in UV and weaker in the optical band. These features can be naturally explained as due to warping of the inner accretion disk (see Chakrabarty et al. 2001). Indeed, using $B \simeq 3 \times 10^{12}$ G (from BeppoSAX observations of a cyclotron feature; Orlandini et al. 1998) and $\dot{M}_{17} \simeq 1$ (corresponding to X-ray luminosity $L_X \simeq 10^{37}$ erg/s; Chakrabarty 1998), eq. (27) yields $\nu_{\text{QPO}} \simeq 0.34 A (\eta/0.5)^{-4.9} \sin^2 \theta \alpha_{-1}^{0.85} \mathcal{J}_{\text{in}}^{-0.7}$ mHz, which can easily give the observed $\nu_{\text{QPO}} = 1$ mHz provided we allow for $\mathcal{J}_{\text{in}} < 1$ [see eq. (29)]. If we interpret the 48 mHz QPO with the BFM, we have $\nu_K(r_{\text{in}}) = 178$ mHz and $\eta \simeq 0.83$, we therefore require $\mathcal{J}_{\text{in}} \lesssim 0.01$ (depending on α and $\sin^2 \theta$).

4.2. Other Sources

For the other sources listed in Table 1, no “smoking-gun” signature of warped disk has been observed. However, the numerical values of QPO frequencies indicate that the MDPM may be at work.

Her X-1: This well-studied binary X-ray pulsar ($\nu_s = 808$ mHz) shows QPOs in the UV and optical bands at frequencies of 8 ± 2 and 43 ± 2 mHz; these QPOs most likely arise from the reprocessing of the disk oscillations by the

companion star (Boroson et al. 2000). A QPO at 12 mHz in X-rays is also present, but its connection with the 8 mHz QPO is not clear (Moon & Eikenberry 2001b). Since $\nu_s > \nu_{\text{QPO}}$, the KFM is not applicable. The BFM predicts $\nu_K(r_{\text{in}}) = 816$ mHz and 851 mHz for $\nu_{\text{QPO}} = 8$ mHz and 43 mHz respectively. For $\mu_{30} \simeq 3$ (see Table 1), $\dot{M}_{17} \simeq 1$ (corresponding to $L_X \simeq 10^{37}$ ergs; Choi et al. 1994), and $M_{1.4} \simeq 1$, we have $\nu_K(r_{\text{in}}) \simeq 400 (\eta/0.5)^{-3/2}$ mHz. Thus to explain the 8 mHz or 43 mHz QPO with the BFM requires $\eta < 0.5$. The phenomenology of the 12 mHz X-ray QPO is consistent with disk precession (see Moon & Eikenberry 2001b); this may be explained by the MDPM.

LMC X-4: This persistent X-ray pulsar ($\nu_s = 74$ mHz) exhibits large X-ray flares. QPOs at frequencies of 0.65–1.35 mHz and 2–20 mHz have been found during such flares (Moon & Eikenberry 2001a). Since $\nu_s > \nu_{\text{QPO}}$, the KFM is not applicable. The BFM predicts $\nu_K(r_m) \simeq 75$ mHz and $\simeq 76$ –94 mHz for $\nu_{\text{QPO}} = 0.65$ –1.35 mHz and 2–20 mHz, respectively. Equation (28) with the measured $\mu_{30} \simeq 11$ (see Table 1) and $\dot{M}_{17} \simeq 25$ (corresponding to $L_X \simeq 5 \times 10^{38}$ ergs; Moon & Eikenberry 2001c) gives $\nu_K(r_{\text{in}}) = 502 (\eta/0.5)^{-3/2}$ mHz, which is much larger than the values of $\nu_K(r_{\text{in}})$ required by the BFM (even for $\eta = 1$). Hence, it is difficult, if not impossible, to identify the observed QPO frequencies (especially for $\nu_{\text{QPO}} = 0.65$ –1.35 mHz) with the beat frequency. On the other hand, eq. (27) gives $\nu_{\text{QPO}} \simeq 1.2 A (\eta/0.5)^{-4.9} \sin^2 \theta \alpha_{-1}^{0.85} \mathcal{J}_{\text{in}}^{-0.7}$ mHz, which is close to the observed $\nu_{\text{QPO}} = 0.65$ –1.35 mHz.

For other sources listed in Table 1, either only single QPO is known, or there is no independent measurement/constraint on μ_{30} and \dot{M} , thus the theoretical interpretation is currently ambiguous.

5. CONCLUSIONS

We have shown in this paper that the inner region of the disk around a strongly magnetized ($\sim 10^{12}$ G) neutron star can be warped and will precess around the stellar spin (see Lai 1999). These effects arise from the interactions between the stellar field and the induced currents in the disk (before it is disrupted at the magnetosphere boundary). We have carried out a global analysis of the warping/precession modes and found that growing modes exist for a wide range of parameters typical of accreting X-ray pulsars. We therefore expect that the magnetically driven warping/precession effect will give rise to variabilities/QPOs in the X-ray/UV/optical fluxes. We have suggested that some mHz QPOs observed in several systems (e.g., 4U 1626-67) are the results of these new magnetic effects. Although there are significant uncertainties in the physical conditions of the magnetosphere-disk boundary [and these uncertainties prohibit accurate calculation of the QPO frequency; see eq. (27)], we emphasize that the existence of these effects is robust. Continued study of the variabilities of X-ray pulsar systems would provide useful constraints on the magnetosphere-disk interactions.

This work is supported in part by NSF Grant AST 9986740, as well as by a research fellowship (to D.L.) from the Alfred P. Sloan foundation.

REFERENCES

Alpar, M. A., & Shaham, J. 1985, *Nature*, 316, 239

Aly, J. J. 1980, *A&A*, 86, 192

Aly, J. J., & Kuippers, J. 1990, *A&A*, 227, 473

Angelini, L., Stella, L., & Parmar, A. N. 1989, *ApJ*, 346, 906

Anzer, U., & Börner, G. 1980, *A&A*, 83, 133

Anzer, U., & Börner, G. 1983, *A&A*, 122, 73

Bardeen, J. M., & Petterson, J. A. 1975, *ApJ*, 195, L65

Boroson, B., et al. 2000, *ApJ*, 545, 399

Campbell, C. G. 1997, *Magnetohydrodynamics in Binary Stars* (Kluwer Academic Pub.: Dordrecht)

Chakrabarty, D. 1998, *ApJ*, 492, 342

Chakrabarty, D., et al. 2001, *ApJ*, in press (astro-ph/0106432)

Choi, C. S., Nagase, F., Makino, F., Dotani, T., & Min, K. W. 1994, *ApJ*, 422, 799

Fendt, C., & Elstner, D. 2000, *A&A*, 363, 208

Finger, M. H., Wilson, R. B., & Harmon, B. A. 1996, *ApJ*, 459, 288

Frank, J., King, A., & Raine, D. 1992, *Accretion Power in Astrophysics* (Cambridge Univ. Press)

Ghosh, P., & Lamb, F. K. 1979, *ApJ*, 234, 296

Ghosh, P., & Lamb, F. K. 1992, in *X-Ray Binaries and Recycled Pulsars*, ed. E. P. J. van den Heuvel & S. A. Rappaport (Dordrecht: Kluwer), p.487

Goodson, A. P., Winglee, R. M., & Böhm, K.-H. 1997, *ApJ*, 489, 199

Grove J. E., et al. 1995, *ApJ*, 438, L25

Hayashi, M. R., Shibata, K., & Matsumoto, R. 1996, *ApJ*, 468, L37

in't Zand, J. J. M., Baykal, A., & Strohmayer, T. E. 1998, *ApJ*, 496, 386

La Barbera, A., Burderi, L., Di Salvo, T., Iaria, R., Robba, N. R. 2001, *ApJ*, in press (astro-ph/0104367)

Lai, D. 1998, *ApJ*, 502, 721

Lai, D. 1999, *ApJ*, 524, 1030

Lamb, F. K., Shibasaki, N., Alpar, M. A., & Shaham, J. 1985, *Nature*, 317, 681

Larwood, J. D., Nelson, R. P., Papaloizou, J. C. B., Terquem, C. 1996, *MNRAS*, 282, L597

Li, J., Wickramasinge, D. T., & Rüdiger, G. 1996, *ApJ*, 469, 765.

Lipunov, V. M., Seménov, E. S., & Shakura, N. I. 1981, *Sov. Astron.*, 25, 439.

Lovelace, R. V. E., Romanova, M. M., & Bisnovatyi-Kogan, G. S. 1995, *MNRAS*, 275, 244.

Lovelace, R. V. E., Romanova, M. M., & Bisnovatyi-Kogan, G. S. 1999, *ApJ*, 514, 368

Makishima, K. 1990, *ApJ*, 365, L59

Makishima, K., & Mihara, T. 1992, in *Proc. Yamada Conf. 28, Frontiers of X-Ray Astronomy*, ed. Y. Tanaka & K. Koyama (Tokyo: Universal Academy), 23

Makishima, K., Mihara, T., Nagase, F., & Tanaka, Y. 1999, *ApJ*, 525, 978

Miller, K. A., & Stone, J. M. 1997, *ApJ*, 489, 890

Moon, D.-S., & Eikenberry, S. S. 2001a, *ApJ*, 549, L225

Moon, D.-S., & Eikenberry, S. S. 2001b, *ApJ*, 552, L135

Moon, D.-S., & Eikenberry, S. S. 2001c, *ApJ*, submitted

Novikov, I. D., & Thorne, K. S. 1973, in *Black Holes*, ed. C. DeWitt & B. DeWitt (New York: Gordon & Breach), 343

Ogilvie, G. I. 1999, *MNRAS*, 304, 557

Ogilvie, G. I., & Dubus, G. 2001, *MNRAS*, 320, 485

Orlandini, M., et al. 1998, *ApJ*, 500, 163

Paul, B., & Rao, A. R. 1998, *A&A*, 337, 815

Papaloizou, J. C., & Pringle, J. E. 1983, *MNRAS*, 202, 1181

Papaloizou, J. C., & Terquem, C. 1995, *MNRAS*, 274, 987

Press, W. H., Teukolsky, S., Vetterling, W. T., & Flannery, B. P. 1992, *Numerical Recipes* (Cambridge: Cambridge Univ. Press)

Pringle, J. E. 1992, *MNRAS*, 258, 811

Pringle, J. E., & Rees, M. J. 1972, *A&A*, 21, 1

Shakura, N. I., & Sunyaev, R. A. 1973, *A&A*, 24, 337

Shinoda, K., Kii, T., Mitsuda, K., Nagase, F., Tanaka, Y., Makishima, K., & Shibasaki, N. 1990, *PASJ*, 42, L27

Shirakawa, A., & Lai, D. 2001, *ApJ*, in press

Shu, F. H., et al. 1994, *ApJ*, 429, 781

Soong, Y., & Swank, J. H. 1989, in *Proc. 23rd ESLAB Symposium on Two Topics in X-ray Astronomy*, ed. N. E. White, J. J. Hunt, & B. Battrick (Paris: ESA), 617

Spruit, H. C., & Taam, R. E. 1993, *ApJ*, 402, 593

Takeshima, T., Dotani, T., Mitsuda, K., & Nagai, F. 1991, *PASJ*, 43, L43

Takeshima, T., Dotani, T., Mitsuda, K., & Nagase, F. 1994, *ApJ*, 436, 871

Terquem, C. E. J. M. L. J. 1998, *ApJ*, 509, 819

Terquem, C., & Papaloizou, J. C. B. 2000, *A&A*, 360, 1031

van Ballegooijen, A. A. 1994, *Space Science Rev.*, 68, 299

van der Klis, M., et al. 1987, *ApJ*, 316, 411

Wang, Y.-M. 1987, *A&A*, 183, 257

Wang, Y.-M. 1995, *ApJ*, 449, L153

Wojdowski, P., Clark, G. W., Levine, A. M., Woo, J. W., & Zhang, S. N. 1998, *ApJ*, 502, 253

TABLE 1
ACCRETION-POWERED X-RAY PULSARS WITH mHz QPOS

System	spin frequency ν_s [mHz]	QPO frequency ν_{QPO} [mHz]	magnetic moment μ_{30} ^b	References ^a
4U 1626-67	130	1, 48	3.3	[1], [2], [3], [4] [†]
Her X-1	807.9	8, 12, 43	3	[5], [6], [7] [†]
SMC X-1	1410	(60) ^c		[8]
Cen X-3	207	35		[9]
LMC X-4	74	0.65–1.35, 2–20	11	[10], [11] [†]
4U 1907+09	2.27	55	2.5	[12], [13] [†]
EXO 2030+375	24	187–213		[14]
4U 0115+63	277	62		[15]
XTE J1858+034	4.5	111		[16]
V 0332+53	229	51	2.5	[17], [18] [†]
A 0535+262	9.71	27–72	9.5	[19], [20] [†]

^aReferences: [1] Shinoda et al. 1990; [2] Chakrabarty 1998; [3] Chakrabarty et al. 2001; [4][†] Orlandini et al. 1998; [5] Boroson et al. 2000; [6] Moon & Eikenberry 2001; [7][†]; Makishima et al. 1999; [8] Wojdowski et al. 1998; [9] Takeshima et al. 1991; [10] Moon & Eikenberry 2001; [11][†] La Barbera et al. 2001; [12] in't Zand et al. 1998; [13][†] Makishima & Mihara 1992; [14] Angelini et al. 1989; [15] Soong & Swank 1989; [16] Paul & Rao 1998; [17] Takeshima et al. 1994; [18][†] Makishima et al. 1990; [19] Finger et al. 1996; [20][†] Grove et al. 1995. These references include QPO discovery (no mark) and magnetic field strength B estimated from cyclotron features (with [†]).

^bThe magnetic moment is calculated by $\mu = BR^3$, or $\mu_{30} = B_{12}R_6^3$. We assume $R = 10$ km, or $R_6 = 1$ here.

^cmarginal detection

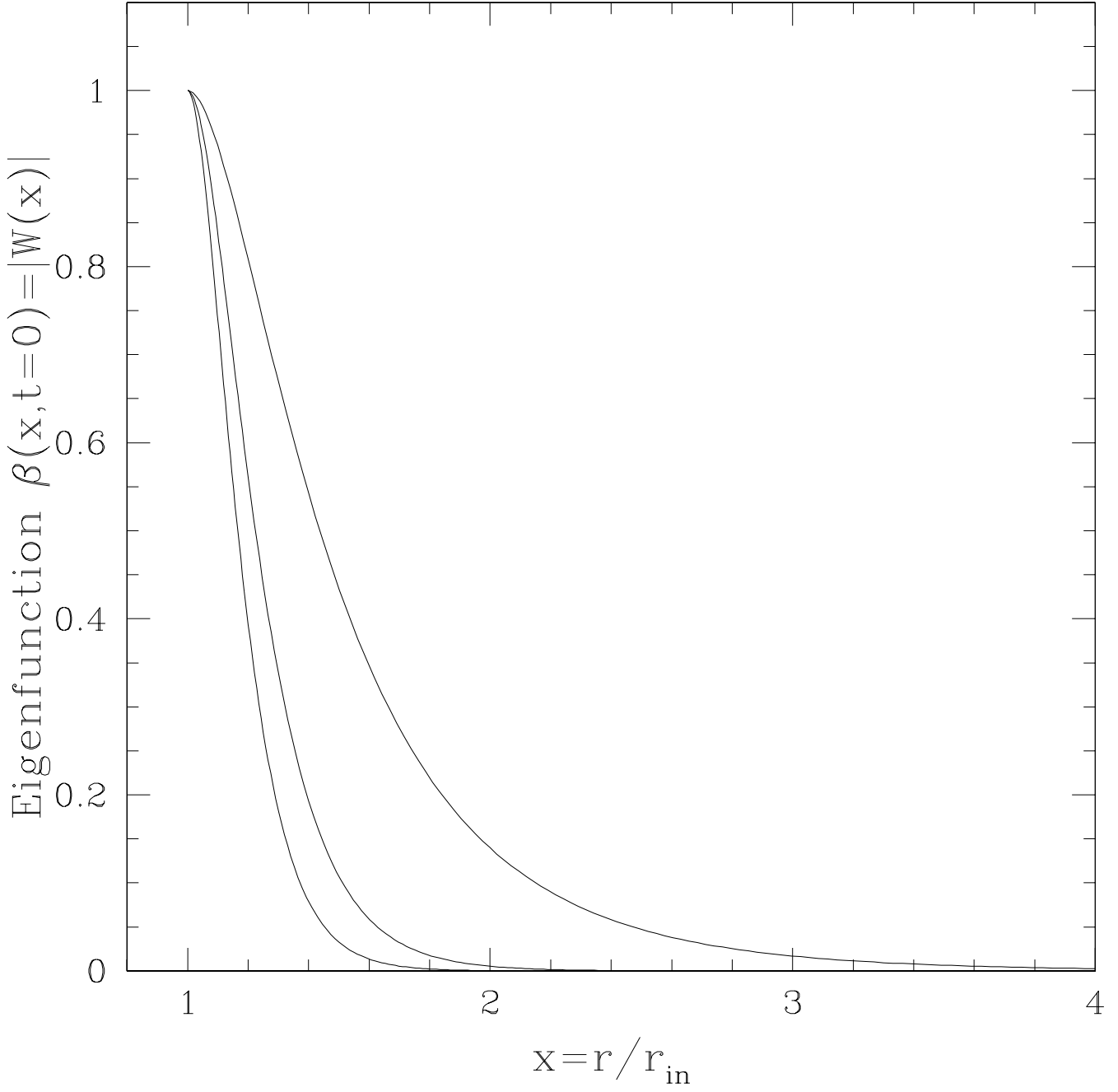


FIG. 1.— The disk tilt angle of the warping/precession modes as determined from eq. (12) with $\mu = -0.6$. The curves represent the fundamental modes for $(\hat{\Omega}_p, \hat{\Gamma}_m) = (-10, 100)$, $(-100, 10)$, and $(-10, 10)$ from left to right, with the corresponding mode frequency $\hat{\sigma} = (\hat{\sigma}_r, \hat{\sigma}_i) = (-6.9, -57)$, $(-62, 12)$, and $(-4.2, -1.7)$. The eigenfunction is normalized such that the maximum tilt angle is 1.

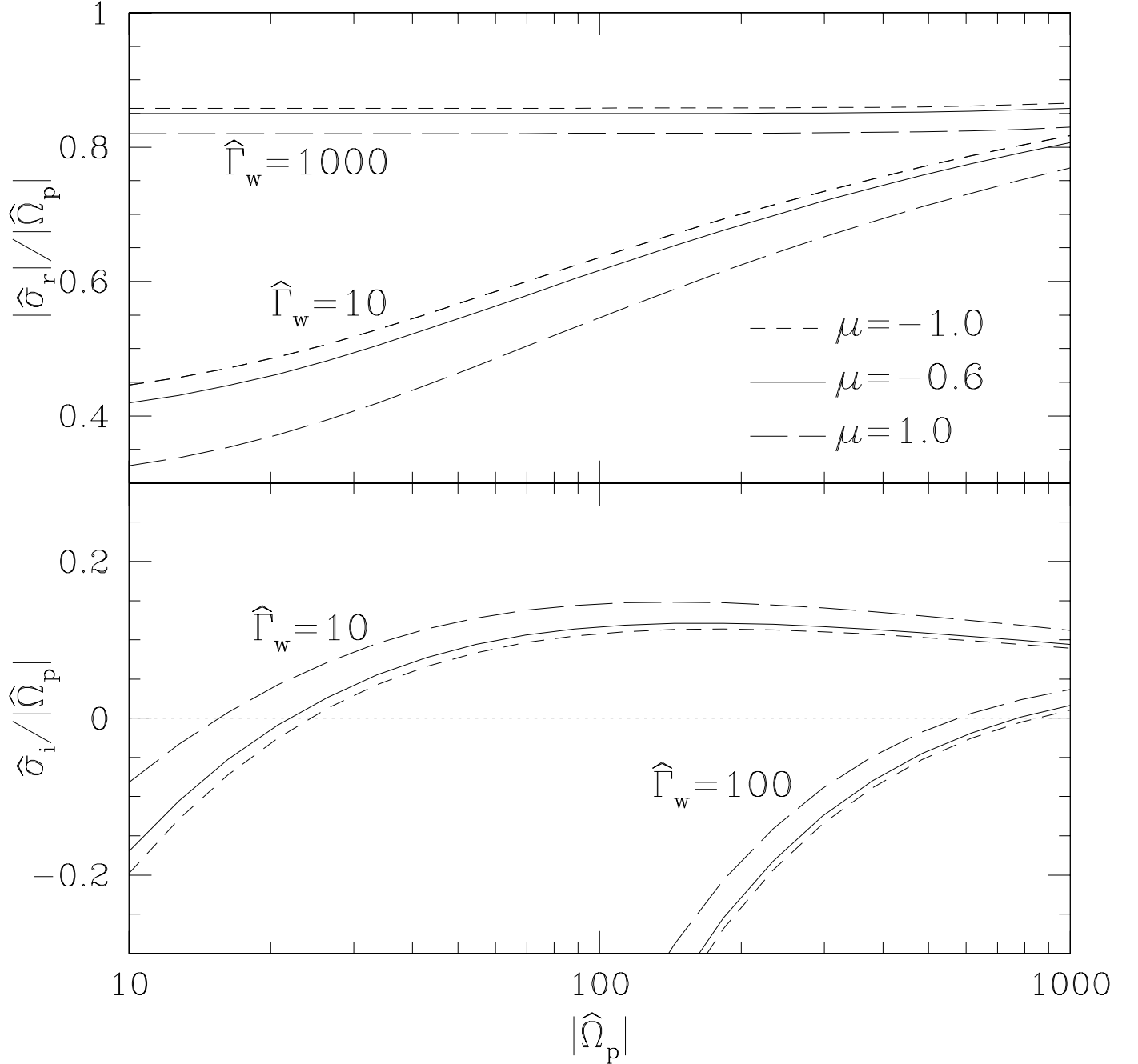


FIG. 2.— The upper panel shows the magnitude of the mode frequency $|\hat{\sigma}_r|$ in units of $|\hat{\Omega}_p|$ as a function of $|\hat{\Omega}_p|$ for different values of $\hat{\Gamma}_w$. Different surface density power-laws, $\Sigma \propto r^\mu$ with $\mu = -1, -0.6$ and 1 , are adopted [see eq. (12)]. The lower panel shows the corresponding mode damping rate $\hat{\sigma}_i$ (in units of $|\hat{\Omega}_p|$). Note that negative $\hat{\sigma}_i$ implies growing mode.

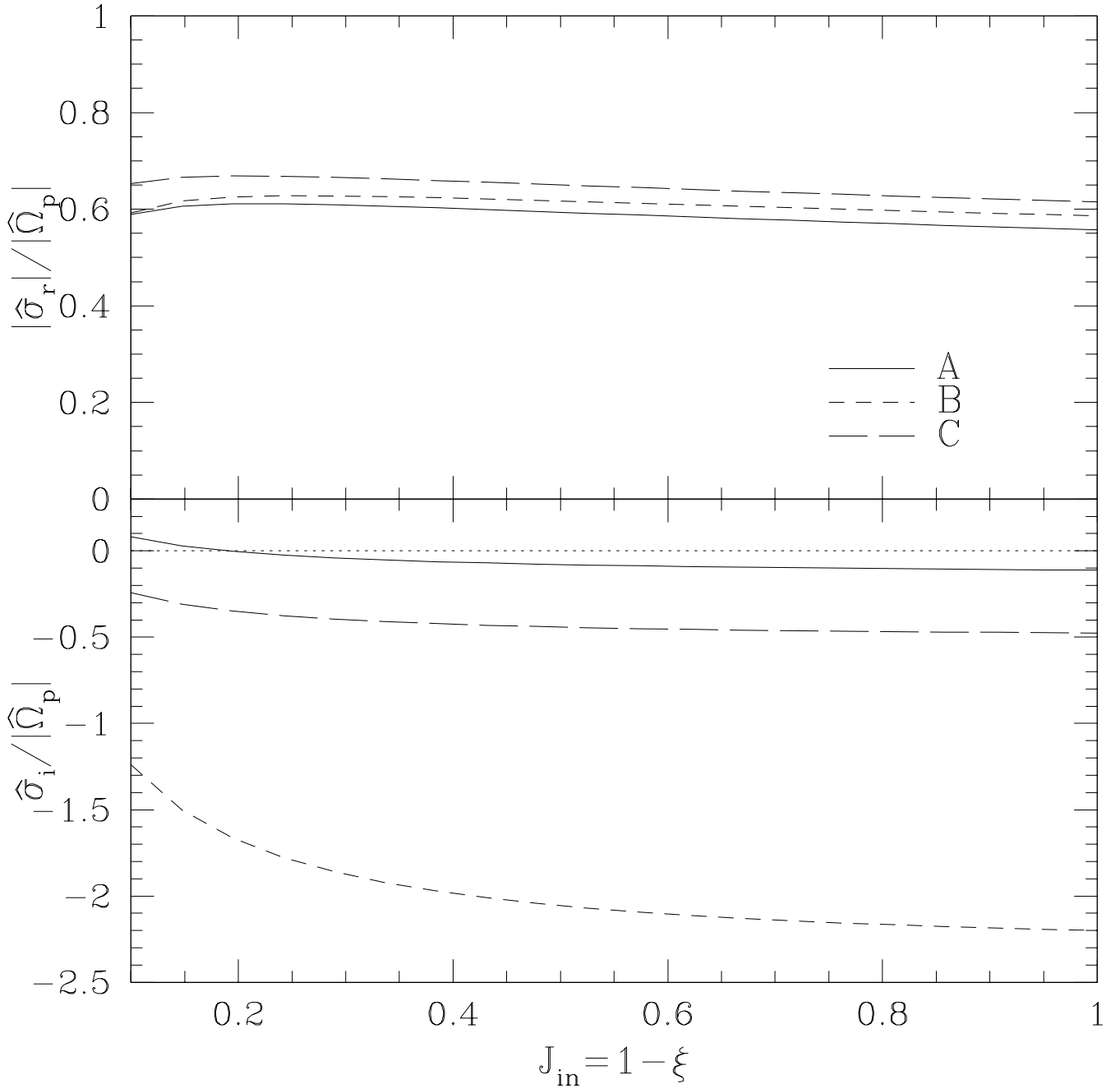


FIG. 3.— The upper panel shows the magnitude of the mode frequency $|\hat{\sigma}_r|$ in units of $|\hat{\Omega}_p|$ as a function of $J_{\text{in}} = 1 - \xi$ for different parameter sets A, B, and C: $(\hat{\Omega}_p, \hat{\Gamma}_w) = (-38J_{\text{in}}^{-1.1}, 21J_{\text{in}}^{-1})$, $(-7.6J_{\text{in}}^{-1.1}, 38J_{\text{in}}^{-1})$, and $(-38J_{\text{in}}^{-1.1}, 43J_{\text{in}}^{-1})$, respectively (see the text). The lower panel shows the corresponding mode damping rate $\hat{\sigma}_i$ (in units of $|\hat{\Omega}_p|$). Note that negative $\hat{\sigma}_i$ implies growing mode.